SOH Estimation Algorithm and Hardware Platform for Lithium-ion Batteries

Mohammad K. Al-Smadi, Student Member, IEEE and Jaber A. Abu Qahouq, Senior Member, IEEE

The University of Alabama Department of Electrical and Computer Engineering Tuscaloosa, Alabama 35487, USA

Abstract—This paper presents a state-of-health (SOH) estimation algorithm and hardware platform for lithium-ion batteries. Based on features obtained from the battery's electrochemical impedance spectroscopy (EIS), an artificial neural network (ANN)-based SOH algorithm is developed. EIS measurements collected at different aging levels are utilized to train and test the SOH estimation algorithm. The minimum impedance magnitude and the impedance magnitude at zero phase show correlations with the battery SOH level and can be utilized to indicate the SOH value. The SOH estimation algorithm performance is evaluated, and the performance evaluation results indicate that the SOH estimation algorithm can be utilized to estimate the SOH.

Keywords—Battery, lithium-ion battery, state of health (SOH), estimation, electrochemical impedance spectroscopy (EIS).

I. Introduction

Lithium-ion battery technology is widely adopted in many applications such as electric vehicles [1, 2], utility-scale energy storage [3], and consumer electronics [4]. To meet the demand for high performance battery systems, developing efficient battery management systems (BMS) became crucial. BMS functions include, but are not limited to, protection, thermal management, and estimation of state of charge (SOC) and state of health [5, 6]. The SOH level (remaining battery capacity) can be utilized to predict early failure of batteries and to trigger protection functions. In addition, it can be used to adjust the charging/discharging strategies to prolong the battery's life [7].

The SOH value can be defined as the ratio between the available battery capacity $Q_{\text{available}}$ and the nominal battery capacity Q_{nominal} (battery capacity when it is new as provided in the manufacturer datasheet) as expressed in (1).

$$SOH = \frac{Q_{available}}{Q_{nominal}} \tag{1}$$

The battery capacity is the amount of charge a fully charged battery can provide as it discharges from its maximum voltage to its minimum voltage. By discharging the battery from its maximum voltage to its minimum voltage, the available capacity $Q_{\text{available}}$ can be obtained.

Various SOH estimation techniques are reported in the literature, and their classifications are based on, but not limited to, the need for direct measurement and whether a physical and/or equivalent circuit models are utilized. Generally, SOH estimation techniques can be classified into model-based techniques and experimental techniques as illustrated in Fig. 1.

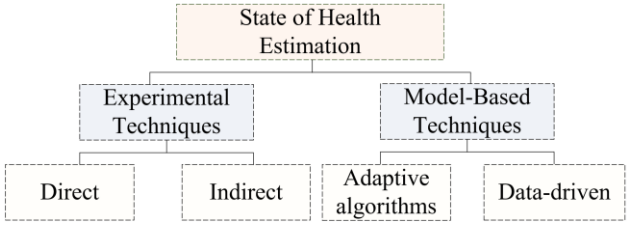


Fig. 1: Battery SOH estimation techniques.

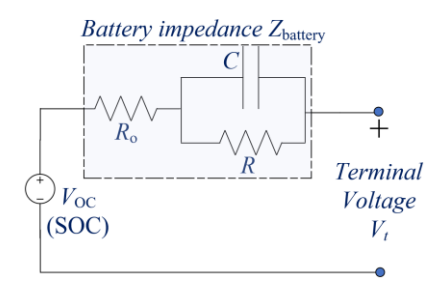


Fig. 2: Simplified equivalent circuit model for a battery.

Experimental SOH estimation techniques are either based on direct measurements (such as Coulomb counting [8] and internal resistance [9]) or indirect analysis (such as incremental capacity analysis and differential voltage analysis [10], and ultrasonic analysis [11]). Model-based techniques are classified into adaptive algorithms (such as Extended Kalman Filter "EKF" [12] and Particle Filter "PF" [13]) and data-driven techniques [14]. Data-driven SOH estimation methods have gained more interest as there is no need to know the underlying aging mechanisms that lead to SOH deterioration [14]. Features extracted from battery historical data (e.gs., charging curves, discharging curves, and impedance) can be utilized to estimate the SOH [14]. Battery impedance spectrum changes (e.g., impedance magnitude increases) as the battery ages and hence can be utilized to estimate the SOH value [15, 16]. Fig. 2 shows a simplified equivalent circuit model (Thevenin model) for a battery. The parameter $V_{\rm OC}$ represents the battery's open circuit voltage and is correlated with the battery SOC level where V_t is the terminal voltage when the battery is under charge/discharge condition. The ohmic resistance is represented by R_0 where the RC parallel branch represents the battery's transient behavior.

This paper presents a data-driven SOH estimator based on some of the features extracted from the battery's electrochemical impedance spectroscopy (EIS). In addition, the architecture of a hardware platform for obtaining EIS measurements and SOH estimation in real-time is presented.

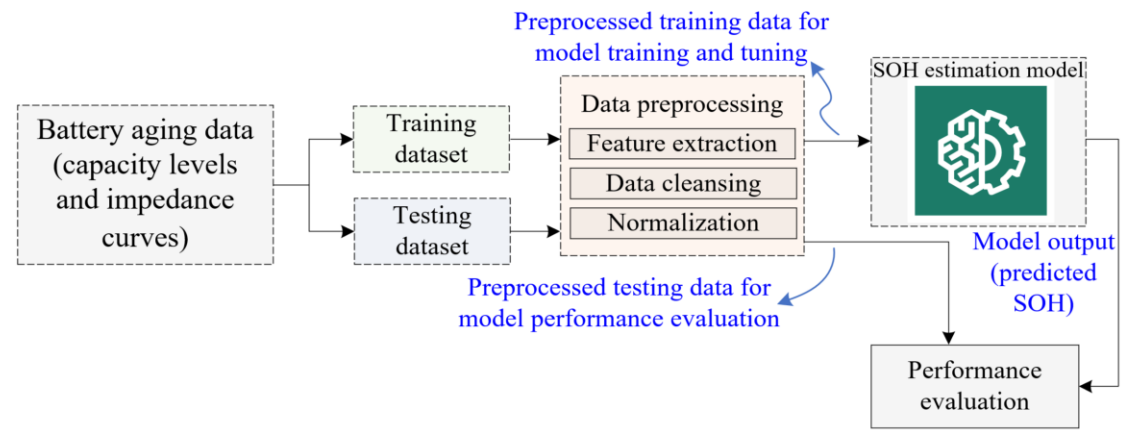


Fig. 4: Overall flowchart of SOH estimation.

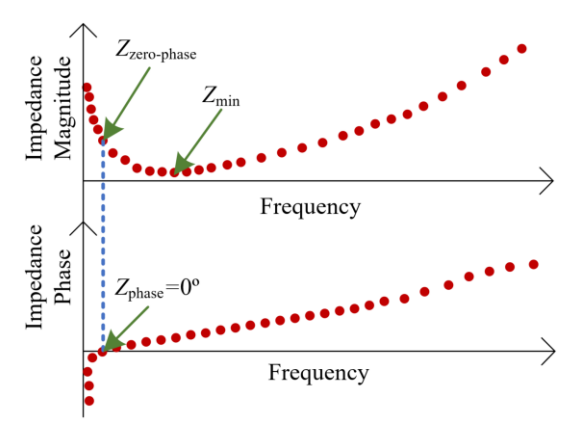


Fig. 3: Typical battery EIS curve with Zmin and Zzero-phase marked.

II. SOH ESTIAMTION ALGORITHM

The SOH estimation algorithm in this paper utilizes some of the features in the battery EIS curve, namely, minimum impedance magnitude Z_{\min} and the impedance magnitude when the impedance phase value is equal to 0° Z_{zero-phase}. Fig. 3 illustrates how both Z_{min} and $Z_{zero-phase}$ can be obtained from a typical EIS curve. Both of these features' values change as the battery ages (as the SOH value decreases). Fig. 5 through Fig. 8 illustrate how each of Z_{min} and $Z_{zero-phase}$ change with SOH value at different state of charge (SOC) levels for two Tenergy ICR 18650 battery cells (nominal capacity C=2.6 Ah [17]) [18]. Both Z_{min} and Z_{zero-phase} values increase as the SOH decreases, showing nonlinear relations. SOH and EIS curves for the two battery cells were obtained from continuous discharging and charging (cycling). Each battery is discharged at 1 C (2.6 A) until the cell voltage reaches the minimum allowable value (2.7 V). The battery cell is charged at constant current (CC) equivalent of a 1 C (2.6 A) until the cell voltage reaches the maximum value (4.2 V). Then, the battery is charged at constant voltage until the battery charging current drops below the end-of-charging current recommended by the manufacturer (50 mA for the battery cells in this paper). Every 30 cycles, the battery capacity is calibrated by measuring the amount of changes (Ah) it provides when discharged from the maximum voltage (4.2 V) to the minimum voltage (2.7 V). Then, the EIS is curve is measured using Gamry 5000E interface potentiostat [19]. The overall flowchart for the SOH estimator presented in this paper is illustrated in Fig. 4. The dataset of one battery (Battery#1) is used for to train the SOH estimator and the dataset of the other battery (Battery#2) is used to test the trained SOH estimator. Different indices are used to evaluate the prediction accuracy of the adopted machine learning algorithm. The following indices are used: root mean square error (RMSE) and mean absolute error (MAE). The two indices are expressed in (3)-(4) where n is the number of the outputs, A(i) is the actual output (true value), and P(i) is the predicted value.

$$RMSE = \sqrt{\frac{1}{n} \sum_{i=1}^{n} (A(i) - P(i))^2}$$
 (3)

$$MAE = \frac{1}{n} \sum_{i=1}^{n} |A(i) - P(i)| \tag{4}$$

Neural network (NN) is utilized to map the nonlinear relationship between the battery health features (Z_{\min} and $Z_{\text{zero-phase}}$) and the battery SOH. Two neural networks were trained and evaluated using the training and testing data at two SOC levels (100% and 60%). The neural networks adopted in this paper include one input layer of 2 inputs, two hidden layers of 5 neurons each, and one output layer. The neural network is trained using deep learning toolbox in Matlab. Mean square error (MSE), expressed in (5) is used as a loss function in the NN training where y(i) is the actual battery SOH in the training dataset and y'(i) is the estimated SOH for the i^{th} training sample. The training algorithm used for the NN training is Levenberg-Marquardt [20].

$$MSE = \frac{1}{n} \sum_{i=1}^{n} |y(i) - \dot{y}(i)|$$
 (5)

After training the NN using Battery#1 data, the parameters of the neural network (which are obtained using the training process), are used to predict the capacity of Battery#2. The prediction accuracy of the trained neural network are then evaluated using the error indices in (3) and (4). The performance evaluation results are summarized in Table I in page 4. The predicted SOH values using the SOH estimator at 100% and 60% SOC levels are plotted against the true SOH values in Fig. 9 and Fig. 10. As shown, the SOH estimator is capable of accurately estimating the SOH value using the input features (Z_{\min} and $Z_{\text{zero-phase}}$).

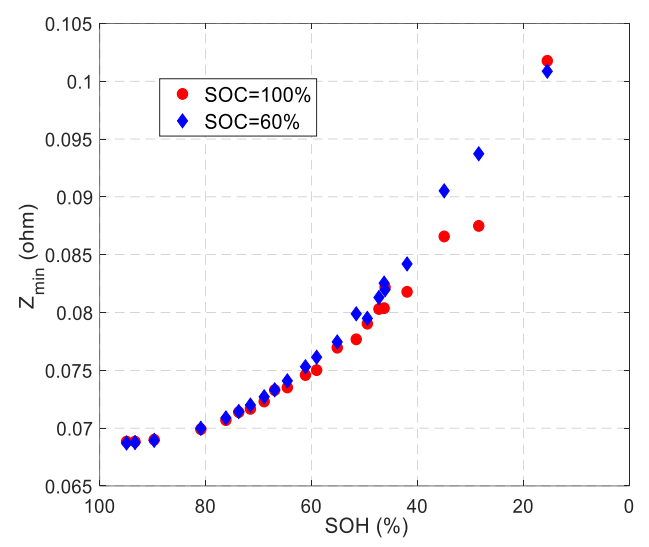


Fig. 5: SOH vs. Z_{min} at different SOC levels for Battery#1.

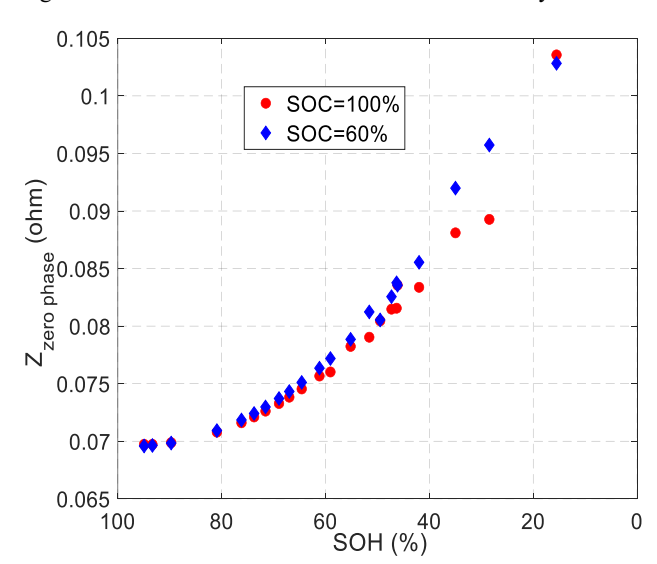


Fig. 6: SOH vs. Z_{zero phase} at different SOC levels for Battery#1.

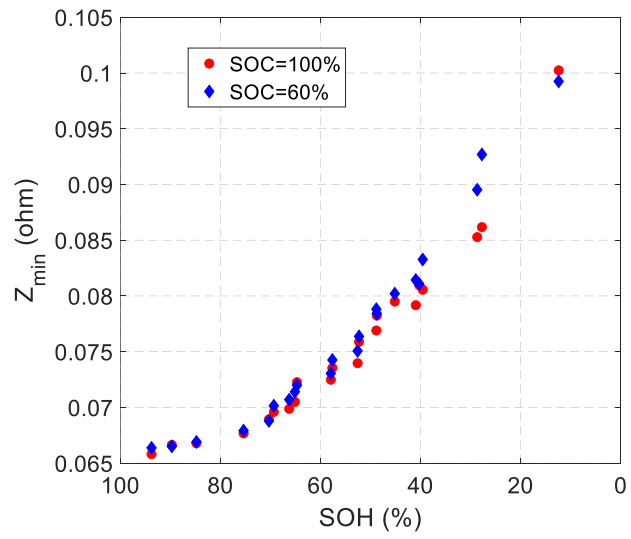


Fig. 7: SOH vs. Z_{min} at different SOC levels for Battery#2.

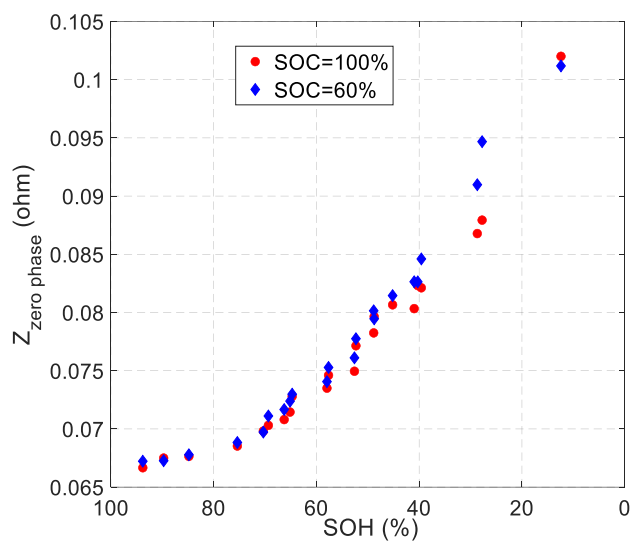


Fig. 8: SOH vs. Zzero phase at different SOC levels for Battery#2.

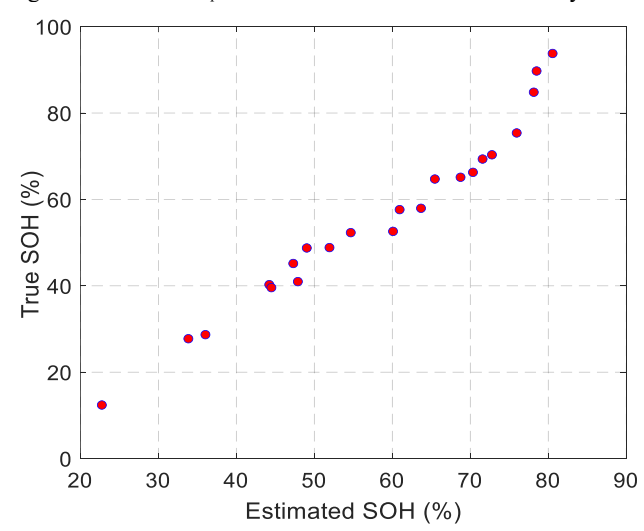


Fig. 9: Estimated SOH vs. True SOH when the SOH estimator is trained and tested using data at SOC=100%.

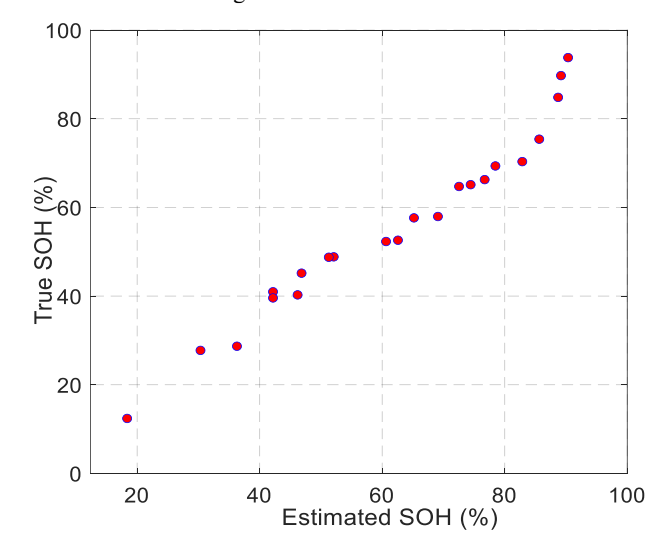


Fig. 10: Estimated SOH vs. True SOH when the SOH estimator is trained and tested using data at SOC=100%

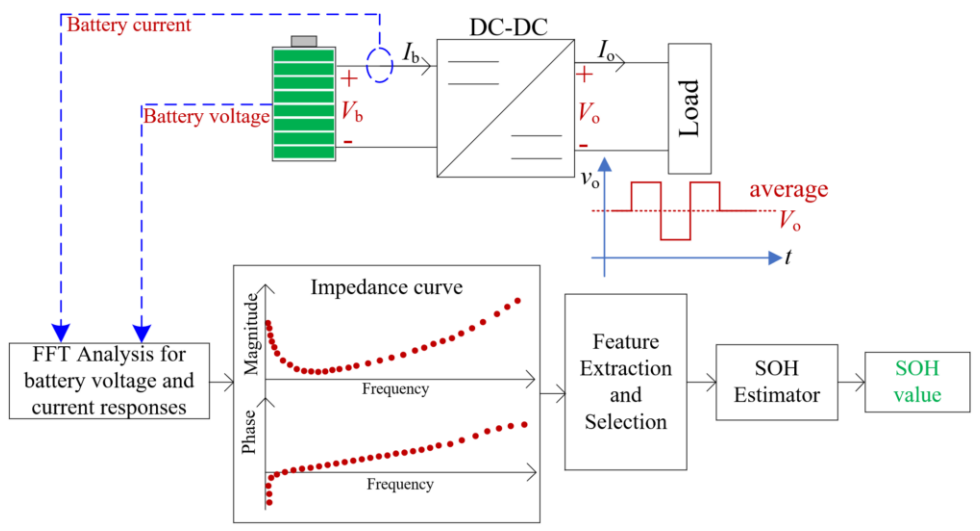


Fig. 11: SOH estimation platform.

Table I: SOH estimator performance

	RMSE	MAE
SOC=100%	0.060	0.050
SOC=60%	0.072	0.063

III. SOH ESTIMATION PLATFORM

To measure the EIS curve while the battery is connected in the system, the online impedance measurement method in [21] is utilized. Fig. 11 shows a block diagram for the SOH platform. The battery is connected to a DC-DC converter whose output voltage is controlled. Perturbing the converter's output voltage V_0 around its reference (average) value results in voltage and current responses at the battery side. Then, Fourier analysis is applied to the battery's voltage and current responses to obtain voltage v_{ac-fo} and current v_{ac-fo} harmonic components which can be used to calculate the impedance magnitude and phase at the frequency v_{ac-fo} at which the converter's output voltage is perturbed as expressed in (6) where v_{ac-fo} is the impedance phase at the frequency v_{ac-fo} By perturbing the converter's output at different frequency values, the EIS spectrum can be obtained

$$Z_{fo} = \frac{v_{ac-f_o}}{i_{ac-f_o}} e^{j\theta_{z-f_o}} \tag{6}$$

Then, SOH features obtained from the EIS curve (Z_{min} and $Z_{zero-phase}$ in this paper) are extracted and fed into the pre-trained NN to estimate the battery SOH value. Conclusion

IV. CONCLUSION

This paper presented a SOH estimation algorithm for lithium-ion batteries. The SOH estimators utilizes features extracted from the battery's impedance curve (minimum impedance magnitude value and the impedance magnitude value when the impedance phase is equal to zero) to estimate the SOH value. The performance of the presented SOH estimation algorithm is evaluated and it shows that the selected features from the battery impedance curve can be utilized for battery SOH estimation.

ACKNOWLEDGEMENT

This material is based upon work supported in part by the National Science Foundation under Grant No. 2213918. Any opinions, findings and conclusions or recommendations expressed in this material are those of the authors and do not necessarily reflect the views of the National Science Foundation.

REFERENCES

- [1] X. Chen, W. Shen, T. T. Vo, Z. Cao, and A. Kapoor, "An overview of lithium-ion batteries for electric vehicles," in 2012 10th International Power & Energy Conference (IPEC), 2012: IEEE, pp. 230-235.
- [2] A. G. Olabi et al., "Battery electric vehicles: Progress, power electronic converters, strength (S), weakness (W), opportunity (O), and threats (T)," *International Journal of Thermofluids*, vol. 16, p. 100212, 2022/11/01/2022, doi: https://doi.org/10.1016/j.ijft.2022.100212.
- [3] H. Zhu et al., "Energy Storage in High Variable Renewable Energy Penetration Power Systems: Technologies and Applications," CSEE Journal of Power and Energy Systems, vol. 9, no. 6, pp. 2099-2108, 2023, doi: 10.17775/CSEEJPES.2020.00090.
- [4] Y. Liang et al., "A review of rechargeable batteries for portable electronic devices," *InfoMat*, vol. 1, no. 1, pp. 6-32, 2019.
- [5] M. K. Al-Smadi and J. A. Abu Qahouq, "Evaluation of Current-Mode Controller for Active Battery Cells Balancing With Peak Efficiency Operation," *IEEE Transactions on Power Electronics*, vol. 38, no. 2, pp. 1610-1621, 2023, doi: 10.1109/TPEL.2022.3211905.
- [6] Y. Cao and J. A. Abu Qahouq, "Hierarchical SOC Balancing Controller for Battery Energy Storage System," *IEEE Transactions on Industrial Electronics*, vol. 68, no. 10, pp. 9386-9397, 2021, doi: 10.1109/TIE.2020.3021608.
- [7] Z. Xia and J. A. Abu Qahouq, "State-of-Charge Balancing of Lithium-Ion Batteries With State-of-Health Awareness Capability," *IEEE Transactions* on *Industry Applications*, vol. 57, no. 1, pp. 673-684, 2021, doi: 10.1109/TIA.2020.3029755.
- [8] K. S. Ng, C.-S. Moo, Y.-P. Chen, and Y.-C. Hsieh, "Enhanced coulomb counting method for estimating state-of-charge and state-of-health of lithium-ion batteries," *Applied Energy*, vol. 86, no. 9, pp. 1506-1511, 2009/09/01/2009, doi: https://doi.org/10.1016/j.apenergy.2008.11.021.
- [9] L. Chen, Z. Lü, W. Lin, J. Li, and H. Pan, "A new state-of-health estimation method for lithium-ion batteries through the intrinsic relationship between ohmic internal resistance and capacity," *Measurement*, vol. 116, pp. 586-595, 2018/02/01/ 2018, doi: https://doi.org/10.1016/j.measurement.2017.11.016.
- [10] E. Schaltz, D.-I. Stroe, K. Nørregaard, L. S. Ingvardsen, and A. Christensen, "Incremental capacity analysis applied on electric vehicles for

- battery state-of-health estimation," *IEEE Transactions on Industry Applications*, vol. 57, no. 2, pp. 1810-1817, 2021.
- [11] X. Li, C. Wu, C. Fu, S. Zheng, and J. Tian, "State characterization of lithium-ion battery based on ultrasonic guided wave scanning," *Energies*, vol. 15, no. 16, p. 6027, 2022.
- [12] C. Hu, B. D. Youn, and J. Chung, "A multiscale framework with extended Kalman filter for lithium-ion battery SOC and capacity estimation," *Applied Energy*, vol. 92, pp. 694-704, 2012.
- [13] T. Wu, S. Liu, Z. Wang, and Y. Huang, "SOC and SOH joint estimation of lithium-ion battery based on improved particle filter algorithm," *Journal of Electrical Engineering & Technology*, vol. 17, no. 1, pp. 307-317, 2022.
- [14] Z. Xia and J. A. Abu Qahouq, "Lithium-ion battery ageing behavior pattern characterization and state-of-health estimation using data-driven method," *Ieee Access*, vol. 9, pp. 98287-98304, 2021.
- [15] Z. Xia and J. A. Abu Qahouq, "Evaluation of Parameter Variations of Equivalent Circuit Model of Lithium-ion Battery under Different SOH Conditions," in 2020 IEEE Energy Conversion Congress and Exposition (ECCE), 11-15 Oct. 2020 2020, pp. 1519-1523, doi: 10.1109/ECCE44975.2020.9236339.
- [16] H.-F. Yuan and L.-R. Dung, "Offline state-of-health estimation for highpower lithium-ion batteries using three-point impedance extraction method," *IEEE Transactions on Vehicular Technology*, vol. 66, no. 3, pp. 2019-2032, 2016.
- [17] Tenergy Corp., Cylindric Lithium-Ion Cell 30005-0, Datasheetof Tenergy, 2010. Accessed: Jul. 19, 2022. [Online]. Available:https://www.shorepowerinc.com/media/wysiwyg/files/Tenergy -30005-0-datasheet.pdf
- [18] Z. Xia and J. A. Abu Qahouq, "Ageing characterization data of lithium-ion battery with highly deteriorated state and wide range of state-of-health," *Data in Brief*, vol. 40, p. 107727, 2022/02/01/ 2022, doi: https://doi.org/10.1016/j.dib.2021.107727.
- [19] Interface 5000ETM potentiostat, Gamry Instruments. [Online]. Available: https://www.gamry.com/potentiostats/interface-5000epotentiostat/.
- [20] J. J. Moré, "The Levenberg-Marquardt algorithm: implementation and theory," in *Numerical analysis: proceedings of the biennial Conference* held at Dundee, June 28–July 1, 1977, 2006: Springer, pp. 105-116.
- [21] J. A. Abu Qahouq and Z. Xia, "Single-Perturbation-Cycle Online Battery Impedance Spectrum Measurement Method With Closed-Loop Control of Power Converter," *IEEE Transactions on Industrial Electronics*, vol. 64, no. 9, pp. 7019-7029, 2017, doi: 10.1109/TIE.2017.2686324.